Nonadiabatic laser-induced orientation and alignment of rotational-state-selected CH_3Br molecules

Sizuo Luo,[1,2] Ruihan Zhu,[3] Lanhai He,[1,2] Wenhui Hu,[1,2] Xiaokai Li,[1,2] Pan Ma,[1,2] Chuncheng Wang,[1,2] Fuchun Liu,[1,2] Wim G. Roeterdink,[1,2] Steven Stolte,[1,2] and Dajun Ding[1,2,*]

[1]*Institute of Atomic and Molecular Physics, Jilin University, Changchun 130012, China*

[2]*Jilin Provincial Key Laboratory of Applied Atomic and Molecular Spectroscopy, Jilin University, Changchun 130012, China*

[3]*School of Science, Changchun University of Science and Technology, Changchun 130022, China*

(Received 21 March 2015; published 11 May 2015)

Nonadiabatic orientation and alignment of hexapole rotational-state-selected methyl bromine (CH_3Br) molecules is studied. The temporal evolution of the mixed dc field and laser-induced orientation and alignment is measured by a pump-probe method. The temporal orientation and alignment transients are in good agreement with the time-dependent Schrödinger equation calculation we perform. We show that the degree of orientation and alignment is strongly dependent on the selected initial rotational state. The temporal transients originating from two different initial states, the $|111\rangle$ state and the mixed $|111\rangle + |212\rangle$ state, are discussed. Our results show a maximum degree of $\langle\cos\theta\rangle = -0.7$ for the orientation of CH_3Br molecules in the $|111\rangle$ state.

DOI: 10.1103/PhysRevA.91.053408 PACS number(s): 37.10.Vz, 32.80.Fb, 42.65.Re, 42.65.Ky

I. INTRODUCTION

The ability to control the orientation and alignment of molecules is an important first step in many contemporary experiments such as imaging of molecular orbitals [1,2] and in reaction dynamics experiments [3]. Unlike in experiments with randomly oriented molecules, the ability to manipulate the angular distribution of molecules makes it possible to obtain molecular frame information [1,2,4,5] and to control physical or chemical processes whose rates are dependent on the orientation of the molecular axis [3,6].

Much effort has been devoted to developing methods that enable control over the orientation and alignment of molecules. The first attempt to experimentally manipulate the angular distribution of molecules was performed about 50 years ago using hexapole electrostatic fields [7]. Rotational-state-selected molecules can be oriented in a moderate uniform static field. Later, a brute-force method was developed to orient molecules with large dipole moments by a strong homogeneous static electric field [8]. This method relies on strong mixing of rotational states in a static electric field. The rapid development of lasers led to many studies that aimed to obtain laser-induced alignment [9–12] and orientation [13–27]. Control of the molecular alignment and orientation can be achieved by nonresonant laser interaction with molecules. Notably, since a pulsed laser can provide a high electric field, adiabatic alignment can be realized when molecules are exposed to a slowly varying laser field with respect to the molecular rotation [9,26]. Nonadiabatic alignment occurs when molecules interact with an ultrafast laser [10–12] and time-dependent alignment revivals appear after the laser pulse has disappeared. The advantage of nonadiabatic alignment is that it can create aligned molecules under field-free conditions where in the case of adiabatic alignment the molecules are only aligned during the presence of the laser pulse.

In general, it is more difficult to create highly oriented molecules as compared to well-aligned molecules. There are two methods to additionally obtain orientation: an all-optical method [13–22] and a method in which a static electric field is combined with a nonresonant laser field [23–27]. The all-optical orientation method employs an asymmetric laser electric field obtained from phase-locked two-color laser fields [13–19] or strong terahertz pulses [20–22]. Phase-locked two-color laser orientation relies on the interaction of the asymmetric laser electric field with the hyperpolarizability of the polar molecule. The terahertz orientation method involves direct rotational excitation enabled by a femtosecond-laser-generated terahertz field that interacts with the molecule's permanent dipole moment. The use of the all-optical orientation method is shown to be a promising route to molecular orientation [19,22]. In order to increase the degree of orientation, rotational state selection of molecules can be used. Holmegaard *et al.* employed a 10-ns Nd:YAG laser pulse to orient and align C_6H_5I molecules after rotational state selection by a molecular deflector, yielding a high orientation in the adiabatic regime [26]. Ghafur *et al.* used a shaped femtosecond laser to nonadiabatically orient NO molecules that were rotational state selected with a hexapole state focuser [27]. This method has proven to be very successful to enhance the degree of orientation since it can provide both a high density of rotational-state-selected molecules and a high degree of orientation.

In the present work we perform a combined experimental and theoretical study on laser nonadiabatic orientation and alignment of CH_3Br molecules. The revivals of both laser-induced orientation and alignment are produced and enhanced significantly by using the rotational-state-selected molecules through a hexapole. The evolutional characteristics of orientation and alignment from different rotational states of molecules have been studied as the result of a unique rotational quantum wave-packet formation.

II. EXPERIMENT

A schematic drawing of the home-built molecular beam machine and the polarizations of the pump (aligning) and probe lasers is shown in Fig. 1. A chirped-pulse-amplified Ti:sapphire laser (Coherent, Libra) is employed to produce a 50-fs linearly polarized laser beam with a repetition rate

*dajund@jlu.edu.cn

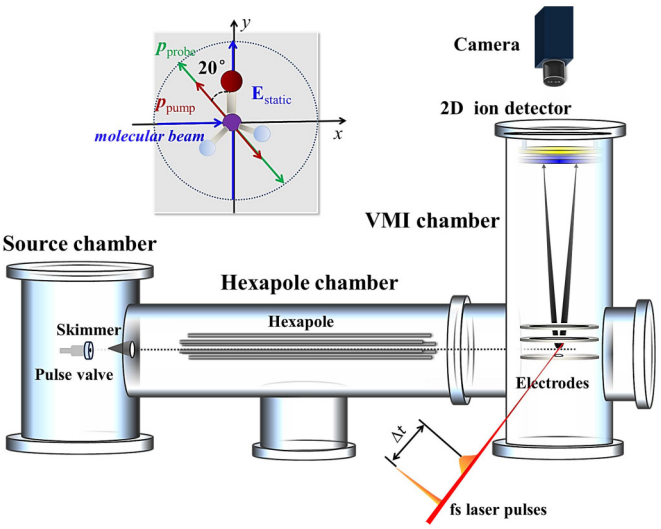

FIG. 1. (Color online) Schematic of the experimental setup. A 300-fs laser pulse (6×10^{12} W/cm^2) is used as the pump for aligning the molecules after rotational state selecting from the hexapole and a 50-fs laser pulse (2×10^{14} W/cm^2) as probe to produce Coulomb explosion of the molecules with a variable delay time with respect to the pump pulse. The polarizations of the pump and probe laser are parallel and are at an angle of 20° with respect to the detector axis (y axis) shown in the inset. The Br^{2+} ion images directly reflect the alignment and orientation of the molecules at the time the probing laser arrived.

of 1 kHz and a 800-nm center wavelength. A Mach-Zehnder interferometer is used to split the laser beam into two parts for a pump-probe measurement. The intensity of each beam is varied by using a half-wave plate and a Glan polarizer. The pump laser pulse is stretched to a width about 300 fs through a block of 70-mm BK7 glass and kept in a region with an intensity to avoid molecular ionization and dissociation. The degree of orientation is measured by the probe laser, which is delayed through a computer-controlled delay stage and is used to Coulomb explode the molecules. By varying the delay time, the temporal evolution of the orientation or alignment is obtained. The pump and probe beams are collinearly focused into the molecular beam by a 250-mm-focal-length lens. The pump laser beam size is reduced using an aperture to ensure that its focus is larger than that of the probe laser. The polarizations of the pump and probe laser are parallel and both are tilted $\alpha = 20^\circ$ with respect to the direction of the static electric field to utilize the combined effect of the pump laser and the static electric field, as shown in Fig. 1.

The apparatus used in the present work consists of three sections: a source, a hexapole, and a velocity-map imaging (VMI) chamber. In the source chamber, a supersonic molecular beam of 2.5% CH_3Br seeded in neon is expanded through a 0.5-mm orifice of a pulsed valve (General Valve Series 9), with a stagnation pressure of 4 bars and a repetition rate of 10 Hz. The hexapole chamber contains six rods with a diameter of 4 mm and a length of 1 m. The inhomogeneous electrostatic field in the hexapole focuses rotational-state-selected molecules into the laser interaction region in the VMI chamber. The spatial orientation of the molecules is measured by Coulomb explosion of molecules in the VMI chamber. The voltages of the VMI repeller and extractor plate are 1000 and 615 V, respectively, producing a static electric field about 260 V/cm in the interaction region of the laser and the molecular beam. The Br^{2+} fragment ions produced from the Coulomb explosion are detected by dual microchannel plates (MCPs) coupled to a fast phosphor screen (P47). To select imaging of the Br^{2+} fragment ions, the MCP is gated by applying a 900-ns voltage pulse (DEI pulse generator) to collect only all the produced Br^{2+} fragments at the specific time of flight. Images of these ions on the phosphor screen are recorded using a CCD camera (Andor iKon-M) and accumulated typically for a few thousand laser shots. Simultaneously the mass spectra can be obtained through monitoring the phosphor screen by a photomultiplier tube connected to a digital storage oscilloscope (Tektronix TDS3054B). All the measured spectra are transferred into a computer for further processing.

III. THEORETICAL METHOD

The interaction of the rotational-state-selected molecules with the intense laser fields has been calculated by solving the time-dependent Schrödinger equation (TDSE) [28–33]. A nonresonant laser interacting with molecules can be described with the following Hamiltonian:

$$H = H_{\rm mol} + H_{\rm ind}, \tag{1}$$

where $H_{\rm mol}$ is the field-free molecular Hamiltonian and $H_{\rm ind}$ is the Hamiltonian describing the laser interaction with the induced dipole moment of the molecules. Employing the rigid-rotor approximation, $H_{\rm mol}$ reduces to the rotational Hamiltonian

$$H_{\rm mol} \approx H_{\rm rot} = \frac{J_x^2}{2I_{xx}} + \frac{J_y^2}{2I_{yy}} + \frac{J_z^2}{2I_{zz}}, \tag{2}$$

where the operators J_k ($k = x,y,z$) are the Cartesian components of the total angular momentum vector and I_{kk} are the corresponding principal moments of inertia. In a nonresonant linearly polarized laser field, the laser cannot interact with the permanent dipole moment and the interaction with the induced dipole moment is well described by the polarizability interaction

$$H_{\rm ind} = -\tfrac{1}{4}\epsilon^2(t)\Delta\alpha\cos^2\theta, \quad \Delta\alpha = \alpha_\parallel - \alpha_\perp \tag{3}$$

in which $\alpha_\parallel = \alpha_{zz}$ and $\alpha_\perp = \alpha_{xx} = \alpha_{yy}$ are the components of polarizability tensor parallel and perpendicular to the molecular axis, respectively. For symmetric top molecules, θ is the angle between the laser field and the molecular symmetric axis and $\epsilon(t)$ is the time profile of the laser field. To solve the time-dependent Schrödinger equation

$$i\hbar\frac{\partial}{\partial t}\Psi(t) = H_{\rm ind}\Psi(t), \tag{4}$$

the wave function is expanded in a suitable basis of rotational states. For symmetric top molecules a suitable basis set consists of the wave functions $|J\,K\,M\rangle$ in which J is the total rotational angular momentum of the molecule, K is the projection of the angular momentum on the symmetry axis of the molecule, and M is the projection of the angular momentum on the direction of the externally applied static electric field. The laser

interaction depends solely on the angle θ, which implies that the quantum numbers K and M are conserved during the laser interaction with the molecules. Therefore, the wave function can be expanded in this complete set of eigenstates

$$|\Psi(t)\rangle = \sum_J C_J(t)|JKM\rangle. \quad (5)$$

Substituting the wave function (5) into the time-dependent Schrödinger equation (4), we obtain the equation for the expansion coefficients $C_J(t)$,

$$i\hbar\frac{\partial}{\partial t}C_J(t) = E_{JK} + \sum_{J'}\langle JKM|H_{\rm ind}|J'KM\rangle \quad (6)$$

$$= E_{JK} - \frac{\Delta\alpha\epsilon^2(t)}{6}\sum_{J'}\langle JKM|D^2_{00}|J'KM\rangle, \quad (7)$$

where E_{JK} is the rotational energy and D^2_{00} is a Wigner rotational matrix [32,33]. In the selected coordinate space, this equation is reduced to a set of first-order ordinary differential equations that can be solved by using a fourth-order Runge-Kutta method [33]. After the laser interaction, the molecules are in a coherent superposition of rotational states and the wave packet evolves freely

$$|\Psi(t)\rangle = \sum_J C_J(t)e^{-iE_{JK}t/\hbar}|JKM\rangle. \quad (8)$$

The time-dependent degree of orientation and alignment can be calculated with

$$\langle\cos\theta\rangle(t) = \langle\Psi(t)|\cos\theta|\Psi(t)\rangle \quad (9)$$

and

$$\langle\cos^2\theta\rangle(t) = \langle\Psi(t)|\cos^2\theta|\Psi(t)\rangle, \quad (10)$$

respectively. It is noteworthy that the solution of the time-dependent Schrödinger equation given by Eq. (8) is a coherent superposition of rotational states that depends on the laser intensity, the polarizability, and the initial rotational state $|JKM\rangle$ of the molecule and pronounced effects have been observed for nonadiabatic orientation and alignment for different initial rotational states of the molecule [12,33,34].

IV. RESULTS AND DISCUSSION

In the hexapole static electric field, an electric field minimum is formed in the center and low-field-seeking molecules experience a force towards this center [7,35–38]. Since the Stark energy depends on the rotational states of the molecule and the gradient of the electric field [7,35], the trajectories of molecules can be controlled by varying the applied rod voltage. For the molecules in a specific rotational state, spatial focusing can be realized at the position where the molecule interacts with the probe laser beam. The measured hexapole focusing curve of CH_3Br is shown in Fig. 2, giving the yield of the parent ion generated in the laser field (4×10^{13} W/cm^2) as a function of the applied voltage. The rotation temperature of the molecular beam is estimated to be 5 K according to a fit of the focusing curve (black line). Due to the spatial focusing, an increase of the molecular beam density is achieved that is typically four times in this experiment. The

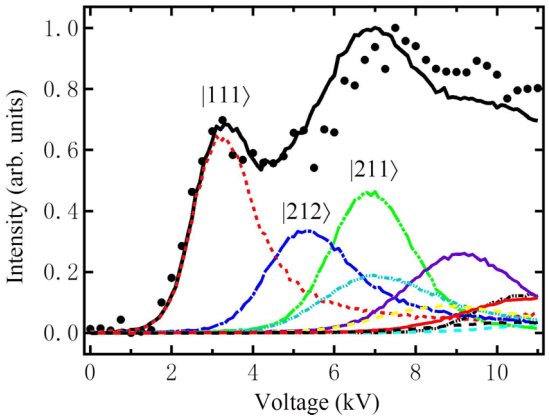

FIG. 2. (Color online) Focusing curve of the CH_3Br molecule seeded in Ne obtained in the experiment from the hexapole focuser. The black circles are the parent ion yield of CH_3Br from a femtosecond laser ionization with an intensity of 4×10^{13} W/cm^2, recorded by the time-of-flight measurement in VMI by a photomultiplier.

specific rotational state that is selected can be identified with the semiclassical trajectories simulation that is described in previous papers [36–38]. The $|111\rangle$ state is selected at 3 kV, which is the first peak in the focusing spectrum. The notation used here actually gives the absolute value for each quantum number (K and M), but the understanding is that the product KM is negative, so the $|111\rangle$ state represents the $|1\text{-}11\rangle$ and $|11\text{-}1\rangle$ states. Increasing the voltage, there are more and more rotational states emerging in the focused molecular beam. Thus, in order to investigate the influence of the quantum wave packet formed from different initial rotational states on orientation and alignment experimentally, we selected two hexapole voltages, 3 and 4.25 kV. At 3 kV the rotational state $|111\rangle$ is selected and at 4.25 kV a mixture of the states $|111\rangle$ and $|212\rangle$ is selected.

We have measured the two-dimensional (2D) velocity distribution of Br^{2+}, produced by the probe laser beam, to observe the revival of the orientation and alignment. The degrees of molecular orientation $\langle\cos\theta_{2D}\rangle$ and alignment $\langle\cos^2\theta_{2D}\rangle$ are defined by the relative intensity of Br^{2+} at different angles. The chosen geometry, where the pump and probe laser polarizations are parallel and make an angle $\alpha = 20^\circ$ with respect to the direction of the electrostatic field, avoids the overlap of the ions from opposite directions at the ion imaging detector. Figures 3(a)–3(d) show the Br^{2+} ion images that are recorded at different pump-probe delay times in the revival for rotational-state-selected $|111\rangle$. Figure 3(a) shows an ion image of the molecules in which the Br atom is initially pointing in the direction of the static electric field. Figure 3(b) shows the orientation of the parent molecule with the Br atom pointing in the opposite direction. This revival rotation continues periodically. The ion image shown in Fig. 3(a) is obtained with a pump-probe delay time of -2 ps, which means that the probe laser interacts with molecules before the pump laser and only a static electric field orientation for the molecules in the rotational state $|111\rangle$ is observed. Increasing the delay time, the high-intensity spot in the Br^{2+} ion image alternates between 180° and 0°. Figure 3(e) shows the measured angular distribution $P(\theta_{2D})$ of the Br^{2+} ions

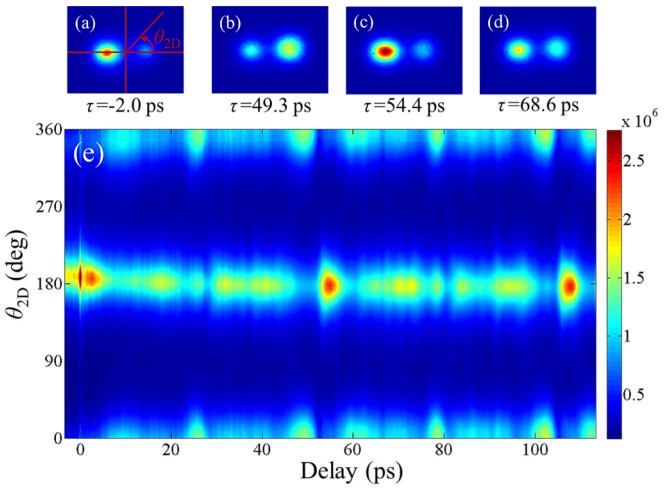

FIG. 3. (Color online) Ion images of Br^{2+} at different delay times (a) $\tau = 2.0$, (b) $\tau = 49.3$, (c) $\tau = 54.4$, and (d) $\tau = 68.6$. (e) Evolution of the measured angular distribution of the Br^{2+} ion imaging given with different delay times and angle θ_{2D}, with respect to the polarization of the probe laser pulse project to the detector plane shown in (a). Here the delay time $t = 0$ represents the instant of time overlap for the pump and probe pulses. All images are taken at rod voltage equal to 3 kV and the rotational state $|111\rangle$ is selected through the hexapole.

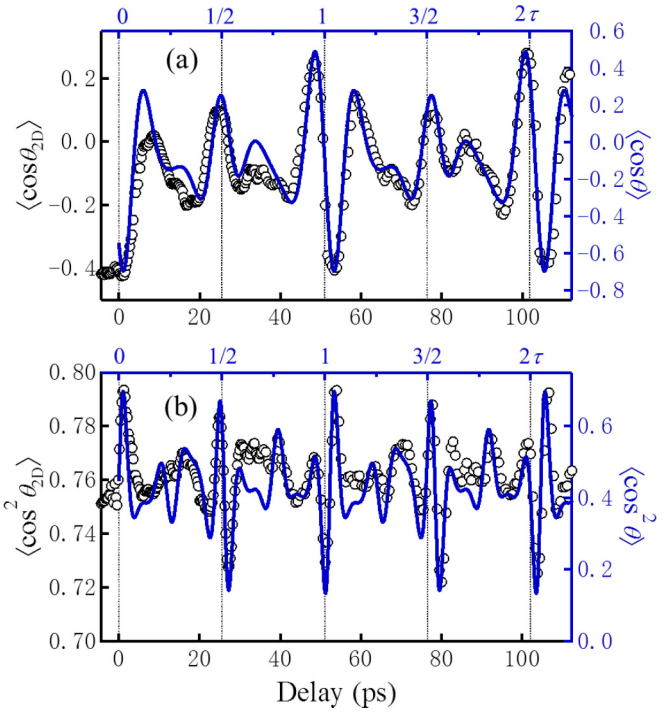

FIG. 4. (Color online) Nonadiabatic evolution of (a) orientation $\langle\cos\theta_{2D}\rangle(t)$ and (b) alignment $\langle\cos^2\theta_{2D}\rangle(t)$ measured from the rotational-state-selected molecular beam ($|111\rangle$ rotational state, black circles). The theoretical results of the orientation $\langle\cos\theta\rangle(t)$ and alignment $\langle\cos^2\theta\rangle(t)$ also are shown (blue lines), obtained by solving the TDSE for a femtosecond laser with an intensity of 6×10^{12} W/cm^2 and pulse duration of 300 fs.

as a function of the pump-probe delay time, where θ_{2D} is the ejection direction with respect to the polarization of the probe laser projected onto the detector plane, as shown in Fig. 3(a). The angular distribution displays a clear inversion when the pump-probe delay time is varied from −4.3 to 112.3 ps. This periodic inversion of the asymmetry parameter indicates that the pump pulse produces an orientational wave packet of CH_3Br molecules. In the time-dependent angular distribution shown in Fig. 3(e), the measured ion yield map captures the revival features of the molecular orientation and alignment. The revival features of Fig. 3(e) originate from a unique rotational wave-packet excitation.

The degrees of orientation $\langle\cos\theta_{2D}\rangle$ and alignment $\langle\cos^2\theta_{2D}\rangle$ and their time evolution are extracted from the measured data shown in Fig. 3(e) and are shown in Figs. 4(a) and 4(b), respectively. These figures also show the TDSE simulation (blue line) for a pump laser intensity of 6×10^{12} W/cm^2. The rotational period of CH_3Br molecules is $\tau = 1/2Bc = 51.76$ ps for a rotational constant $B = 0.322$ cm^{-1}. For the orientational revival [Fig. 4(a)] the measurement gives two full revival periods at a delay time of 112.3 ps. The actual degree of molecular orientation $\langle\cos\theta\rangle$ can be obtained by matching the revival features from the measured evolution to that from the simulation obtained by adjusting the laser intensity. The best agreement between the measured and the calculated evolutions is obtained at the laser intensity of 6×10^{12} W/cm^2, enabling us to get the value of $\langle\cos\theta\rangle = -0.7$ at $t = 53.0$ ps, which corresponds to the measured maximum orientation of $\langle\cos\theta_{2D}\rangle = -0.425$. The discrepancy from the values of $\langle\cos\theta_{2D}\rangle$ and $\langle\cos\theta\rangle$ may originate from the difference of the laboratory and molecular frames, the dynamic and geometric alignment and orientation created by the probe laser, the angle between the pump and probe lasers [27], and the influence from the residual beam not selected by the hexapole field. Similarly, from the measured evolution of the alignment $\langle\cos^2\theta_{2D}\rangle$ shown in Fig. 4(b), the actual value of $\langle\cos^2\theta\rangle = 0.7$ for the degree of alignment can be derived, by the same procedure described above. Strong alignment revivals are observed experimentally with a period of $\tau \approx 52.0$ ps. The maximum degree of alignment occurs at 0, 1, and 2 times the rotational period. Because the polarization of the probe laser is tilted at an angle $\alpha = 20^\circ$ with respect to the static electric field, the measured $\langle\cos^2\theta_{2D}\rangle$ is affected by the geometric alignment of the molecules in the probe laser field, leading to a large difference between the measured and the actual degrees of alignment.

The ability of preparing a molecular beam populated at different rotational states allows us to study the influence of the rotational state on the nonadiabatic orientation and alignment. For a molecular beam populated with both $|111\rangle$ and $|212\rangle$ states, the measured evolution of the orientation $\langle\cos\theta_{2D}\rangle$ and alignment $\langle\cos^2\theta_{2D}\rangle$ is shown in Fig. 5. Differences in the revival characteristics and the degree of orientation and alignment are observed compared to the revivals obtained for the molecules populated in the initial $|111\rangle$ rotational state as in Fig. 4. It is found that the maximum degree of orientation in the case of the mixed quantum state molecular beam is $\langle\cos\theta\rangle = -0.61$ at $t = 54.0$ and 105.3 ps [see Fig. 5(a)]. This is lower than that in the case of the $|111\rangle$ state where $\langle\cos\theta\rangle = -0.7$ [see Fig. 4(a)]. Comparing the revival curves shown in Figs. 5(b) and 4(b), the maximum degree obtained is

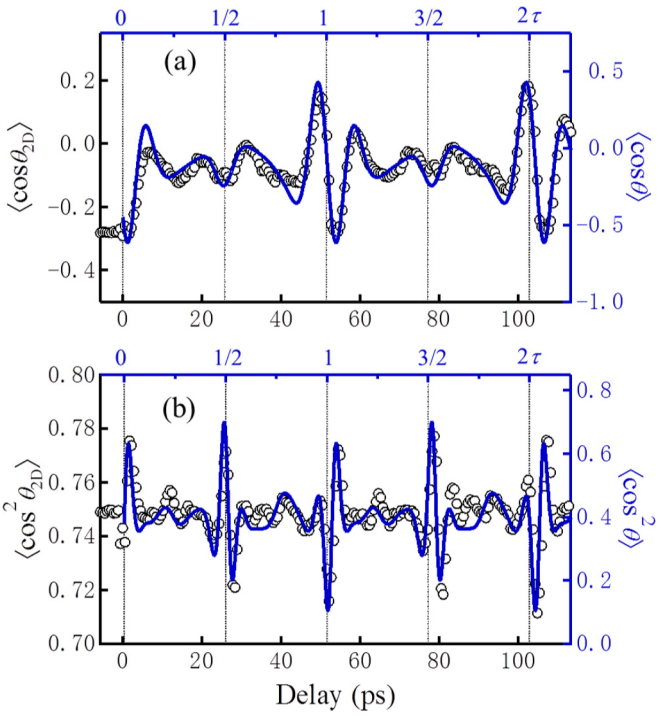

FIG. 5. (Color online) Same as Fig. 4 but for a molecular beam occupied in the mixed rotational states of $|111\rangle$ and $|212\rangle$ (equally populated) for (a) the orientation and (b) the alignment.

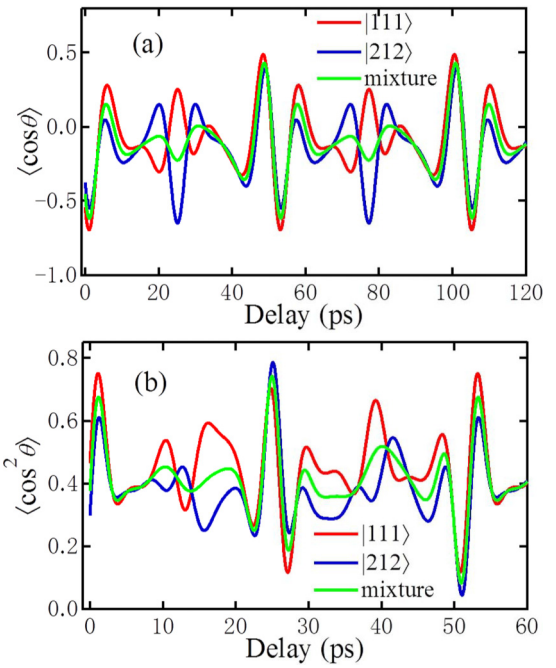

FIG. 6. (Color online) The TDSE calculation results of the evolution for the (a) orientation and (b) alignment from different initial populated states (red, $|111\rangle$ rotational state; blue, $|212\rangle$ state; green line, a mixture of $|111\rangle$ and $|212\rangle$ rotational states).

$\langle\cos^2\theta\rangle = 0.7$ for both situations, but the maximum degree of alignment is obtained at $t = 1/2\,\tau, 3/2\,\tau$ for the mixed beam and $t = \tau, 2\,\tau$ for the $|111\rangle$ rotational state.

The theory for the formation of a rotational wave packet from laser excitation has been discussed before [28–32] and the effect of the initial rotational state on the formed wave packet and the orientation and alignment dynamics has been reported [12,33]. In the present experiment, the evolution of the rotational wave packet shows a rapidly changing value of the orientation and alignment during a few picoseconds (see Figs. 4 and 5). For example, at the delay time of 49.3 ps the value of the orientation $\langle\cos\theta_{2D}\rangle$ is positive, indicating that the Br atom points in the opposite direction to the static electric field, but at a delay time of 54.0 ps the value of the orientation becomes negative and the Br atom points in the direction of the static electric field. Rapid revivals are also observed in the evolution of the alignment. These changes directly reflect the molecular movement that is controlled by the rotational wave packet formed during the pump laser excitation. It is found that different revival structures appear when we measure the evolutions of the orientation and alignment originating from different initial states. A clear difference is observed at $t = 1/2\,\tau, 3/2\,\tau$ for the orientation between the single and mixed states [see Figs. 4(a) and 5(a)]. For the alignment, at $t = 1/4\,\tau, 3/4\,\tau, 5/4\,\tau, 7/4\,\tau$ a difference is also observed [see Figs. 4(b) and 5(b)]. The revival structures at quarters of the revival period ($1/4\,\tau$ and $3/4\,\tau$) are out of phase for the odd and even rotational states [39–41]. Thus, with the odd and even rotational states unequally populated, as in Fig. 4(b) for the $|111\rangle$ initial state, a sharp alignment peak is observed at these times. However, with equally or close to equally populated even and odd rotational states, the revival structures from the two parities superimpose destructively and the revival structures at $1/4\,\tau$ and $3/4\,\tau$ are suppressed, as is evident from Fig. 5(b) for the $|111\rangle$-$|212\rangle$ mixture. These nonadiabatic revival features of the quantum rotational wave packet observed are perfectly simulated by our numerical TDSE calculation. It shows clearly the difference between the evolution of the orientation and alignment from the molecules populated in different rotational states $|111\rangle$ and $|212\rangle$ (red and blue curves, respectively, in Fig. 6). We also plotted the curve of the statistical average (green curve) in Fig. 6 by assuming an equal population in both states $|111\rangle$ and $|212\rangle$, which corresponds to the experimentally derived populations at a hexapole voltage of 4.25 kV without including the contribution of the direct beam. In Fig. 6(a) the evolutions of the orientation from the initial states $|111\rangle$ (red) and $|212\rangle$ (blue) show opposite behavior around $1/2\,\tau$ and $3/2\,\tau$, leading to a destructive superposition in the total revival curve (green) for the mixed beam. This effect is seen also in the alignment [see Fig. 6(b)]. For example, the revival around $1/4\,\tau$ and $3/4\,\tau$ of the mixed beam is lower than that of the revival structure of the $|111\rangle$ state because of destructive superposition. The delay time t at which the maximum degree of alignment is observed is different for the rotational states $|111\rangle$ and $|212\rangle$, i.e., $t \approx \tau$ for the maximum from the $|111\rangle$ state and $t \approx 1/2\,\tau$ for that originating from the $|212\rangle$ state, which is in agreement with the experimental observation. Consequently, the differences in the evolution of the orientation and alignment indicate the distinctions of the rotational wave packets formed from femtosecond laser excitation of different initial rotational states $|111\rangle$ and $|212\rangle$. This is experimental observation of the influence of initial states on the evolution of nonadiabatic orientation and alignment of CH_3Br molecules.

V. CONCLUSION

A combined experimental and theoretical study of nonadiabatic orientation and alignment of quantum-state-selected symmetric top CH_3Br molecules has been carried out and the influence of the initial rotational-state populations is investigated. The technique used in the present work enables us to control the orientation and alignment of CH_3Br molecules. A comparative study of the nonadiabatic evolution of the orientation and alignment from different initial rotational states, i.e., $|111\rangle$ and $|212\rangle$, has been presented. A maximum degree of orientation $\langle\cos\theta\rangle = -0.7$ for CH_3Br molecules prepared in the $|111\rangle$ rotational state is obtained. It is found that the degree and the evolutional behavior of the orientation and alignment are strongly affected by the initial state population of the molecules. The nonadiabatic orientation and alignment of quantum-state-selected molecules give deep insight into the mechanisms of these processes in ultrafast laser fields and provide an elaborate method to manipulate the molecular orientation that can be used in a wide range of molecular frame studies.

ACKNOWLEDGMENTS

This work was supported by the National Basic Research Program of China (973 Program) through Grant No. 2013CB922200 and the National Natural Science Foundation of China (Grants No. 11034003, No. 1127403, and No. 91221301).

[1] J. Itatani, J. Levesque, D. Zeidler, H. Niikura, H. Pepin, J. C. Kieffer, P. B. Corkum, and D. M. Villeneuve, Nature (London) **432**, 867 (2004).
[2] J. B. Bertrand, H. J. Wörner, P. Salières, D. M. Villeneuve, and P. B. Corkum, Nat. Phys. **9**, 174 (2013).
[3] C. Vallance, Phys. Chem. Chem. Phys. **13**, 14427 (2011).
[4] D. Pavicic, K. F. Lee, D. M. Rayner, P. B. Corkum, and D. M. Villeneuve, Phys. Rev. Lett. **98**, 243001 (2007).
[5] J. Yao, G. Li, X. Jia, X. Hao, B. Zeng, C. Jing, W. Chu, J. Ni, H. Zhang, H. Xie, C. Zhang, Z. Zhao, J. Chen, X. Liu, Y. Cheng, and Z. Xu, Phys. Rev. Lett. **111**, 133001 (2013).
[6] X. Xie, K. Doblhoff-Dier, H. L. Xu, S. Roither, M. S. Schöffler, D. Kartashov, S. Erattupuzha, T. Rathje, G. G. Paulus, K. Yamanouchi, A. Baltuška, S. Gräfe, and M. Kitzler, Phys. Rev. Lett. **112**, 163003 (2014).
[7] K. H. Kramer and R. B. Bernstein, J. Chem. Phys. **42**, 767 (1965).
[8] J. C. Loison, A. Durand, G. Bazalgette, R. White, E. Audouard, and J. Vigue, J. Chem. Phys. **99**, 13591 (1995).
[9] H. Stapelfeldt and T. Seideman, Rev. Mod. Phys. **75**, 543 (2003).
[10] F. Rosca-Pruna and M. J. J. Vrakking, Phys. Rev. Lett. **87**, 153902 (2001).
[11] C. Wu, G. Zeng, Y. Gao, N. Xu, L. Peng, H. Jiang, and Q. Gong, J. Chem. Phys. **130**, 231102 (2009).
[12] J. H. Nielsen, P. Simesen, C. Z. Bisgaard, H. Stapelfeldt, F. Filsinger, B. Friedrich, G. Meijer, and J. Küpper, Phys. Chem. Chem. Phys. **13**, 18971 (2011).
[13] J. Wu and H. Zeng, Phys. Rev. A **81**, 053401 (2010).
[14] S. Zhang, C. Lu, T. Jia, Z. Wang, and Z. Sun, Phys. Rev. A **83**, 043410 (2011).
[15] K. Oda, M. Hita, S. Minemoto, and H. Sakai, Phys. Rev. Lett. **104**, 213901 (2010).
[16] S. De, I. Znakovskaya, D. Ray, F. Anis, N. G. Johnson, I. A. Bocharova, M. Magrakvelidze, B. D. Esry, C. L. Cocke, I. V. Litvinyuk, and M. F. Kling, Phys. Rev. Lett. **103**, 153002 (2009).
[17] M. Spanner, S. Patchkovskii, E. Frumker, and P. Corkum, Phys. Rev. Lett. **109**, 113001 (2012).
[18] I. Znakovskaya, M. Spanner, S. De, H. Li, D. Ray, P. Corkum, I. V. Litvinyuk, C. L. Cocke, and M. F. Kling, Phys. Rev. Lett. **112**, 113005 (2014).
[19] X. Ren, V. Makhija, H. Li, M. F. Kling, and V. Kumarappan, Phys. Rev. A **90**, 013419 (2014).
[20] C. Shu, K. Yuan, W. Hu, and S. Cong, J. Chem. Phys. **132**, 244311 (2010).
[21] S. Fleischer, Y. Zhou, R. W. Field, and K. A. Nelson, Phys. Rev. Lett. **107**, 163603 (2011).
[22] K. N. Egodapitiya, S. Li, and R. R. Jones, Phys. Rev. Lett. **112**, 103002 (2014).
[23] H. Sakai, S. Minemoto, H. Nanjo, H. Tanji, and T. Suzuki, Phys. Rev. Lett. **90**, 083001 (2003).
[24] H. Tanji, S. Minemoto, and H. Sakai, Phys. Rev. A **72**, 063401 (2005).
[25] A. Goban, S. Minemoto, and H. Sakai, Phys. Rev. Lett. **101**, 013001 (2008).
[26] L. Holmegaard, J. H. Nielsen, I. Nevo, H. Stapelfeldt, F. Filsinger, J. Küpper, and G. Meijer, Phys. Rev. Lett. **102**, 023001 (2009).
[27] O. Ghafur, A. Rouzee, A. Gijsbertsen, W. K. Siu, S. Stolte, and M. J. J. Vrakking, Nat. Phys. **5**, 289 (2009).
[28] T. Seideman, J. Chem. Phys. **103**, 7887 (1995).
[29] B. Friedrich and D. Herschbach, Phys. Rev. Lett. **74**, 4623 (1995).
[30] M. Leibscher, I. S. Averbukh, and H. Rabitz, Phys. Rev. Lett. **90**, 213001 (2003).
[31] M. Leibscher, I. S. Averbukh, and H. Rabitz, Phys. Rev. A **69**, 013402 (2004).
[32] E. Hamilton, T. Seideman, T. Ejdrup, M. D. Poulsen, C. Z. Bisgaard, S. S. Viftrup, and H. Stapelfeldt, Phys. Rev. A **72**, 043402 (2005).
[33] R. Zhu, C. Wang, S. Luo, X. Yang, M. Zhang, F. Liu, and D. Ding, Front. Phys. **8**, 236 (2013).
[34] J. Ortigoso, M. Rodríguez, M. Gupta, and B. Friedrich, J. Chem. Phys. **110**, 3870 (1999).
[35] R. W. Anderson, J. Phys. Chem. A **101**, 7664 (1997).
[36] F. Liu, M. Jin, X. Gao, and D. Ding, Chin. Phys. Lett. **23**, 344 (2006).
[37] F. Liu, M. Jin, and D. Ding, Chin. Phys. Lett. **23**, 1165 (2006).
[38] W. G. Roeterdink, J. Bulthuis, E. P. F. Lee, D. Ding, and C. A. Taatjes, Chem. Phys. Lett. **598**, 96 (2014).
[39] M. Renard, E. Hertz, B. Lavorel, and O. Faucher, Phys. Rev. A **69**, 043401 (2004).
[40] S. Fleischer, Y. Khodorkovsky, E. Gershnabel, Y. Prior, and I. S. Averbukh, Isr. J. Chem. **52**, 414 (2012).
[41] P. W. Dooley, I. V. Litvinyuk, K. F. Lee, D. M. Rayner, M. Spanner, D. M. Villeneuve, and P. B. Corkum, Phys. Rev. A **68**, 023406 (2003).